Computer-Assisted Intramedullary Nailing Using Real-Time Bone Detection in 2D Ultrasound Images

Agnès Masson-Sibut[1,2], Amir Nakib[1], Eric Petit[1], and François Leitner[2]

[1] Laboratoire d'Images Signaux et Systémes Intelligents (EA 3945), Université Paris Est Créteil, Créteil, France
[2] Research Center, Aesculap SAS, Echirolles, France
agnes.masson-sibut@bbraun.com, amir.nakib@u-pec.fr, eric.petit@u-pec.fr, francois.leitner@bbraun.com

Abstract. In this paper, we propose a new method for bone surface detection in 2D ultrasound (US) images, and its application in a Computer Assisted Orthopaedic Surgery system to assist the surgeon during the locking of the intramedullary nail in tibia fractures reduction. It is a three main steps method: first, a vertical gradient is applied to extract potential segments of bone from 2D US images, and then, a new method based on shortest path is used to eliminate all segments that do not belong to the final contour. Finally, the contour is closed using least square polynomial approximation. The first validation of the method has been done using US images of anterior femoral condyles from 9 healthy volunteers. To calculate the accuracy of the method, we compared our results to a manual segmentation performed by an expert. The Misclassification Error (ME) is between 0.10% and 0.26% and the average computation time was 0.10 second per image.

Keywords: 2D ultrasound, bone surface, segmentation, Computer Assisted Surgery.

1 Introduction

In Computer Assisted Orthopaedic Surgery (CAOS) systems, the intra-operative image modality of choice is often Computed Tomography (CT) or fluoroscopy (X-rays projection). These image modalities are not completely safe for patients and users because they produce ionized radiations. Within the last decade, ultrasounds (US) became a valuable alternative for orthopaedic surgeons. Ultrasound devices are not too expensive, and portable. Also, ultrasound imaging can be used in real-time intra-operatively and it is non-invasive. However, the US images are difficult to analyze for the surgeon because of the high level of attenuation, shadow, speckle and signal dropouts [1].

In the literature, the extraction of the bone surface in US images was studied by Heger *et al.* [2]. The authors used an A-mode ultrasound pointer. The

K. Suzuki et al. (Eds.): MLMI 2011, LNCS 7009, pp. 18–25, 2011.

probe was tracked mechanically to register the distal femur in total hip replacement. The A-mode of ultrasound probes consists in using the representation of the signal amplitude for one line in the tissue. Usually, the B-mode is preferred by surgeons, since the output is an image representing the brightness of the US response for several lines in the tissue. In CAOS systems, US imaging can be used to collect some sample landmarks on bone surface [3], or to perform intra-operative registration, extracting the full 3D model of an anatomical structure [4]. Manual segmentation of the bone surface in US images is highly operator dependent and time consuming [5]. Moreover, the thickness of the bone surface can reach 4 mm in some images [1], so manual segmentation can lead to an error higher than some millimeters. Foroughi *et al.* [6] developed an automatic segmentation method of bone surface in US images using dynamic programming. This method depends on a threshold value. The obtained average error was between 2.10 pixels to 2.67 pixels at the comparison between automatic and manual segmentation ; the average time of computation per image was 0.55 seconds.

In this paper, our main interest lies on the use of US images in computer assisted intramedullary nailing of tibia shaft fractures. If a surgeon chooses to reduce a tibia shaft fracture using an intramedullary nail, then he has to lock the nail in the bone. Normand *et al.* proposed to use some measures on the healthy symmetric tibia to assist the surgeon during the locking of the nail [7]. The authors noticed that the locking of the intramedullary nail without assistance can lead to important modifications in the orientation or the length of the broken tibia. They suggested using the healthy symmetrical tibia as model to assist the surgeon during the locking. Then, the broken bone could be reconstructed identical to its symmetrical. The proposed system used 3D positions of some anatomical landmarks (malleolus, trochlea, femoral condyles, ...) on both the broken and the healthy tibia to calculate their length and orientation, and the healthy tibia should not be injured. Then, the authors proposed to use the US probe as a percutaneous pointer (Fig. 1). Our work focuses on the development of a new method to extract the bone surface in real-time in order to find automatically anatomical landmarks.

The proposed method consists in three main steps. In the first step, a vertical gradient is applied to extract potential segments of the bone from 2D US images. In the second step, a new method based on a shortest path algorithm is used to eliminate all segments that do not belong to the final contour. Finally, the contour is closed using polynomial interpolation.

The rest of the paper is organized as follows: in Section 2, the proposed method is presented. Then, we show and discuss the obtained results in Section 3. The conclusion is in Section 4.

2 Proposed Method

Let $I : \Omega \subset \mathbb{N}^2 \rightarrow \mathcal{I} \subset \mathbb{N}$ be an image (two dimensional (2D) real function). Segmenting bone surface in I consists in extracting $\{P_i | i = 1, .., n\}$ a subset of contiguous points in I, where $P_i = (x_i, y_i) \in \Omega, \forall i = 1, .., n$. Considering

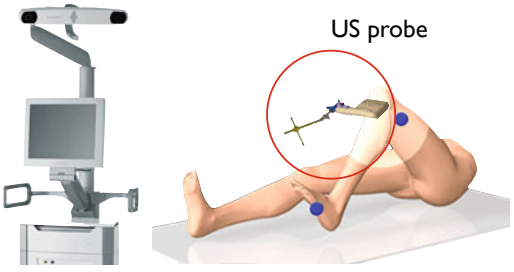

(a) (b)

Fig. 1. Illustration of the CAOS system to assist the surgeon during the locking of the nail. (a) The station used to track the US probe. (b) Position of the patient during the US acquisition of anterior femoral condyles.

ultrasound properties of bones [1], we admit that $\forall(i,j) \in [1,n]^2$ such that $i \neq j$, we have $y_i \neq y_j$.

Then, the proposed segmentation method consists in three steps: in the first step, original images are filtered, a vertical gradient is computed, and an extraction of some potential segments of bone contour is performed. Then, the second step consists in characterizing these segments of contour, in order to eliminate those that *a priori* do not belong to the bone contour. Final step consists in closing the contour using least square polynomial approximation.

2.1 Preprocessing Step

Ultrasound images are highly textured, mainly with speckle. Then, the first substep of preprocessing is to apply a low-pass filter to the original image in order to eliminate noise and to strengthen interesting features. To find the best low pass filter, a frequency analysis of the different sequences by hand was done. We tested empirically several low-pass filters: Gaussian filters were too permissive but a good noise attenuation was found using a circular averaging filter. Once the filtered image I_s is computed, the vertical gradient is applied to it, and we denote the result image I_g (Fig. 2.(b)). The choice of the vertical gradient is motivated by ultrasound propagation properties, where the bone contours are mainly horizontal. It was shown in [1] that the bone contour is likely to lie in the top of the US bone response. Then, we only keep high values of the gradient.

To isolate the high values of the gradient, we need to threshold I_g (Fig. 2.(c)). In order to get a threshold that is independent of the image parameters (contrast, ...), we propose to use the cumulative histogram $\mathcal{H}_{cum}$ of gradient values which is defined by:

$$\mathcal{H}_{cum}(x) = \sum_{i=1}^{x} h(x),\ \forall x = 1,..,N\Delta q \tag{1}$$

where $h(x)$ is the histogram value at the gradient level x of I_g, N is the number of levels in gradient values, and Δq is the step between two levels. We define the

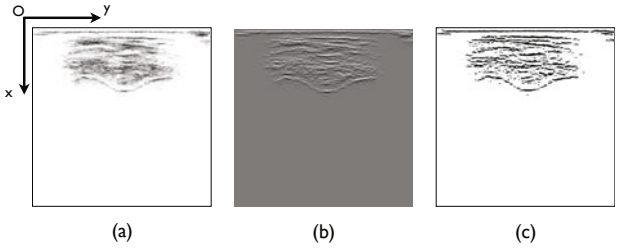

Fig. 2. Illustration of the preprocessing step method. In order to improve the visibility of US images, the grey levels are inverted. (a) Inverted initial image. (b) Gradient image. (c) Thresholded image.

optimal threshold (p) for I_g that expresses the percentage of low gradient values that have to stay at "0". Here, we define $p = 0.95$. Then,

$$I_{BW} = \begin{cases} 1 & \text{if } I_g > t \text{ where } t = \mathcal{H}_{cum}^{-1}(p \times \mathcal{H}_{cum}(N\Delta q)) \\ 0 & \text{otherwise} \end{cases} \tag{2}$$

Using properties of ultrasound imaging of bones [1], we can extract from I_{BW} a first subset of potential contour points $\{Q_i | i = 1, .., c\}$, where c is the number of columns in I. Considering that we can have at most one Q_i per column, contour points are denoted $Q_i = (x_i, i), \forall i = 1, .., c$ in the rest of the paper. The subset of Q_i is built by taking the lowest non-zero point in each column of I_{BW}:

$$Q_i(I) = \begin{cases} argmax\{k | I_{BW}(k, i) \neq 0\} \\ 0, \text{ if } argmax = \emptyset \end{cases} \quad \forall i = 1, .., c \tag{3}$$

The next step consists in characterizing these points to determine whether or not they belong to the bone contour.

2.2 False Alarm Elimination

The subset of points $\{Q_i | i = 1, .., c\}$ (Fig. 3.(a)) are potentially part of the bone contour. To select those that belong to the bone contour, we consider them as segments by grouping contiguous points. Two points are considered to be contiguous if they belong to the same 3x3 neighborhood. In this step, we assume that segments smaller than 5 pixels correspond to noise, so they are eliminated. Those closer than 50 pixels to the top of the image are also eliminated because they are too close to the skin. For each segment k, where $k = 1, .., M$, the first point is designated by Q_{a_k} and the last point by Q_{b_k}, where a_k and b_k are the column of Q_{a_k} and Q_{b_k} respectively.

To define segments that belong to the bone contour, we define $\mathcal{G}(\mathcal{N}, \mathcal{E})$ as an oriented graph, using the M segments (Figure 4):

$$\begin{aligned} \mathcal{N} &= \{n_i \mid i = 1, .., 2M\} \\ &= \{a_k \mid k = 1, .., M\} \cup \{b_k \mid k = 1, .., M\} \end{aligned} \tag{4}$$

(a) (b)

Fig. 3. Illustration of the false alarm elimination step. (a) Potential contour points before the false alarm elimination. (b) Remaining points after the Dijkstra algorithm.

is the set of all nodes in the graph, where the node index n_i is defined by:

$$\forall i \in [1, 2M], \quad n_i = \begin{cases} a_{\frac{i+1}{2}} & \text{if } i \text{ is odd} \\ b_{\frac{i}{2}} & \text{if } i \text{ is even} \end{cases} \tag{5}$$

We define also the set of edges in the graph as: $\forall (i,j) \in [1, 2M]^2$,

$$\mathcal{E}(i,j) = \begin{cases} \frac{1}{2}(b_{\frac{j}{2}} - a_{\frac{j}{2}}) & \text{if } i \text{ is odd and } j = i+1 \\ \|Q_{b_{\frac{i}{2}}} - Q_{a_{\frac{j+1}{2}}}\| & \text{if } i \text{ is even, } j \text{ is odd, and } i < j < min(2M, i+6) \\ 0 & \text{otherwise} \end{cases} \tag{6}$$

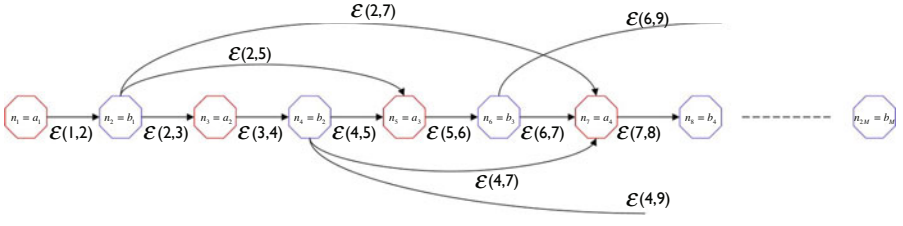

Fig. 4. The construction of the graph $\mathcal{G}$. We distinguish nodes called *"start of segments"* which are the a_k nodes and the nodes called *"end of segments"* which are the b_k nodes.

The graph $\mathcal{G}$ contains two types of nodes: nodes *start-of-segments*, which are $\{a_k \,|\, k = 1, ..., M\}$ with a single child (b_k), and the weight of corresponding edges is $\frac{1}{2}(b_{\frac{j}{2}} - a_{\frac{j}{2}})$, and, the nodes *end-of-segments* which are $\{b_k \,|\, k = 1, ..., M\}$ with at most three children which are $\{a_l \,|\, l = k+1, ..., min(k+3, M)\}$, and the weight of corresponding edges are $\|Q_{b_{\frac{i}{2}}} - Q_{a_{\frac{j+1}{2}}}\|$. The intra-segment edges values are penalized to enforce inter-segment distance as driving force and are considered in the computation of the global shortest path.

Then, Dijkstra's algorithm [8] is used to find the shortest path between the node n_1 and the node n_{2M} in the oriented graph $\mathcal{G}$. An illustration of the obtained result after the application of Dijkstra algorithm is presented Figure 3.(b).

2.3 Contour Closure

The closure of the contour is performed by a polynomial approximation using least square method. The approximation is calculated on the m points that belong to the final set of segments. The degree of the polynomial has been defined empirically by $R = 10 < m$ in order to have a unique solution. An illustration of the closure is given in Figure 5.

Fig. 5. Illustration of the contour closure

3 Results

To illustrate the effectiveness of the method, different tests were performed on several series of US images. The probe and the beamformer were provided by Telemed (Vilnius, Lituania), and the acquisition software was developed by Aesculap SAS (Echirolles, France) using the Software Development Toolkit provided by Telemed. The acquisition parameters were a frequency at 7 MHz and two focus points at 20 mm and 34 mm. The acquisition protocol consists in locking the probe under the patella, and performing a scan of the femoral condylar region rotating the probe up and down. To test the proposed method, a database for 29 men and women, from 24 to 61 year-old, was used. The results presented here are on 230 US images from 9 representative volunteers from this database.

To qualify the final segmentation, the Root Mean Square Error (RMSE) and Misclassification Error (ME) [9] measures were used to compare the obtained results to an expert's segmentation. After outliers elimination, the maximal value of the RMSE is around 7 pixels ($\approx$ 0.8mm) which is quite good considering that the acceptable error is around 2mm in a CAOS applications. The ME values between 0.10% and 0.26% illustrate the accuracy of the method comparing to the expert's segmentation. The algorithm was tested on Matlab R2008a and runs at 10-15 images per seconds, which can be considered as a real-time in our context.

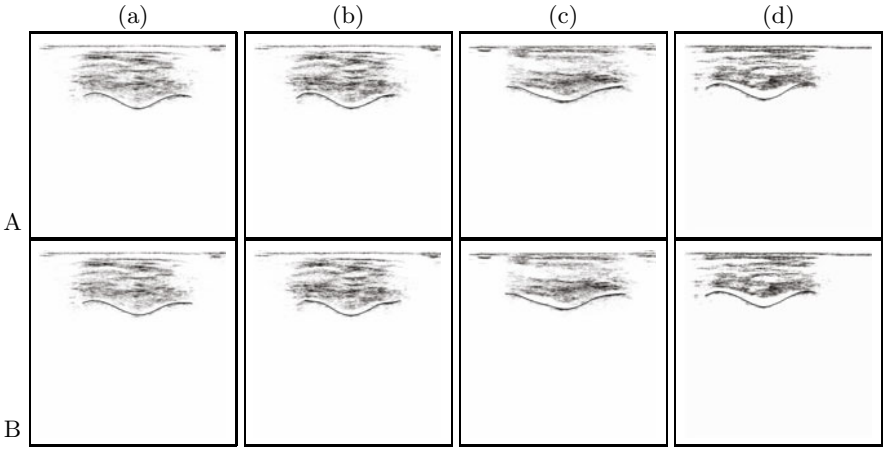

Fig. 6. Comparison between the expert's segmentation and the automatic segmentation for images from 4 different volunteers. A.(a)(b)(c)(d) Results of the expert's segmentation. B.(a)(b)(c)(d) Results of the automatic segmentation.

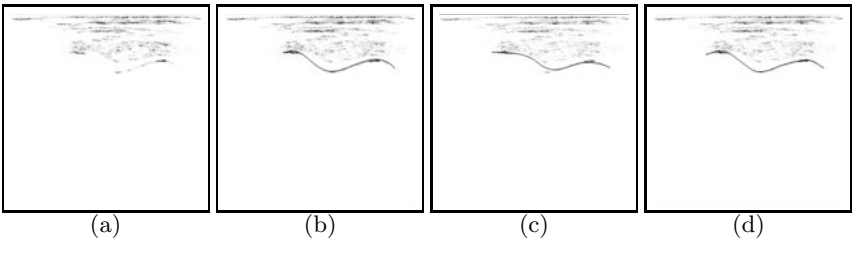

Fig. 7. Illustration of the comparison between segmentation result using an active contour, and the proposed method. (a) Original US image. (b) US image segmented by an expert. (c) US image segmented using an active contour model. (d) US image segmented using the proposed method.

Figure 6 shows some results: the first line represents the results of the expert's segmentation, and the second line represents the results given by the automatic segmentation. The difference between them is not visually significant.

The obtained results of the proposed method were compared to those obtained by the snake based method described in [10]. The comparison is illustrated in Figure 7. The RMSE value between the segmentation result of the snake based method and the manual segmentation is 14.4 pixels (11.5mm).

4 Conclusion

In this paper, a new method of condyles detection in ultrasound images was presented. The method took into account both ultrasounds, and bones properties

to have the best final result. We tested the method on 230 images, with the same acquisition parameters. First results are very promising, especially in our context of application: its use in a CAOS system to assist the surgeon during intramedullary nailing of tibia shaft fractures.

Nevertheless, automatic interpretation of US images is non trivial: images of the same organ can vary a lot depending on the patient, and on the set of parameters used for the acquisition. In future work, a study on the settings of the acquisition parameters will be done.

In work under progress, to improve the quality of the segmentation, a geometric a priori of the condyles contour is added.

References

1. Jain, A.K., Taylor, R.H.: Understanding bone responses in B-mode ultrasound images and automatic bone surface extraction using a Bayesian probabilistic framework. In: Proceedings of International Conference SPIE Medical Imaging, vol. 5373, pp. 131–142. Spie, Bellingham (2004)
2. Heger, S., Portheine, F., Ohnsorge, J., Schkommodau, E., Radermacher, K.: User-interactive registration of bone with A-mode ultrasound. IEEE Engineering in Medicine and Biology Magazine 24, 85–95 (2005)
3. Beek, M., Abolmaesumi, P., Luenam, S., Sellens, R.W., Pichora, D.R.: Ultrasound-guided percutaneous scaphoid pinning: Operator variability and comparison with traditional fluoroscopic procedure. In: Larsen, R., Nielsen, M., Sporring, J. (eds.) MICCAI 2006. LNCS, vol. 4191, pp. 536–543. Springer, Heidelberg (2006)
4. Zhang, Y., Rohling, R., Pai, D.: Direct surface extraction from 3D freehand ultrasound images. In: Proceedings of the Conference on Visualization 2002, p. 52. IEEE Computer Society, Boston (2002)
5. Barratt, D.C., Penney, G.P., Chan, C.S.K., Slomczykowski, M., Carter, T.J., Edwards, P.J., Hawkes, D.J.: Self-calibrating 3D-ultrasound-based bone registration for minimally invasive orthopedic surgery.. IEEE Transactions on Medical Imaging 25, 312–323 (2006)
6. Foroughi, P., Boctor, E., Swartz, M.J., Taylor, R.H., Fichtinger, G.: Ultrasound Bone Segmentation Using Dynamic Programming. In: 2007 IEEE Ultrasonics Symposium Proceedings, pp. 2523–2526. IEEE, New York (2007)
7. Normand, J., Harisboure, A., Leitner, F., Pinzuti, J., Dehoux, E., Masson-Sibut, A.: Experimental navigation for bone reconstruction. In: 10th Annual Meeting of The International Society for Computer Assisted Orthopaedic Surgery Proceedings, Versailles, France (2010); Poster 39
8. Dijkstra, E.W.: A note on two problems in connexion with graphs. Numerische Mathematik 1, 269–271 (1959)
9. Sezgin, M., Sankur, B.: Survey over image thresholding techniques and quantitative performance evaluation. Journal of Electronic Imaging 13, 146–165 (2004)
10. Kass, M., Witkin, A., Terzopoulos, D.: Snakes: Active contour models. International Journal of Computer Vision 1, 321–331 (1988)